Journal of Materials Chemistry

Cite this: *J. Mater. Chem.*, 2012, **22**, 10119

www.rsc.org/materials

FEATURE ARTICLE

Synthetic routes toward MOF nanomorphologies

Erik A. Flügel,[ab] Annekathrin Ranft,[ab] Frederik Haase[ab] and Bettina V. Lotsch*[ab]

Received 5th November 2011, Accepted 17th January 2012
DOI: 10.1039/c2jm15675j

As metal–organic frameworks (MOFs) are coming of age, their structural diversity, exceptional porosity and inherent functionality need to be transferred into useful applications. Fashioning MOFs into various shapes and at the same time controlling their size constitute an essential step toward MOF-based devices. Moreover, downsizing MOFs to the nanoscale triggers a whole new set of properties distinguishing nanoMOFs from their bulk counterparts. Therefore, dimensionality-controlled miniaturization of MOFs enables the customised use of nanoMOFs for specific applications where suitable size and shape are key prerequisites. In this feature article we survey the burgeoning field of nanoscale MOF synthesis, ranging from classical protocols such as microemulsion synthesis all the way to microfluidic-based techniques and template-directed epitaxial growth schemes. Along these lines, we will fathom the feasibility of rationally designing specific MOF nanomorphologies—zero-, one- and two-dimensional nanostructures—and we will explore more complex "second-generation" nanostructures typically evolving from a high level of interfacial control. As a recurring theme, we will review recent advances made toward the understanding of nucleation and growth processes at the nanoscale, as such insights are expected to further push the borders of nanoMOF science.

1. Introduction

Coordination chemistry has lived through a renaissance with the discovery of highly porous, crystalline framework materials composed of metal ions or clusters joined by rigid, polytopic organic linkers.[1,2] The triumphant success and rapid growth of this class of hybrid materials, dubbed metal–organic frameworks (MOFs) or porous coordination polymers (PCPs), are largely based on their elegant yet simple synthesis and their versatility originating from the use of tailorable linkers and the resulting high surface areas and porosities. Although the validity of rational MOF synthesis is not universal and some doubt has been cast recently on the viability of true secondary building-block approaches,[3] MOF chemistry continues to intrigue by offering

[a]*Max Planck Institute for Solid State Research, Heisenbergstraße 1, 70569 Stuttgart, Germany. E-mail: b.lotsch@fkf.mpg.de; Fax: +49-711-689-1612*
[b]*Department of Chemistry and Center for NanoScience (CeNS), University of Munich (LMU), Butenandtstrasse 5-13 (D), 81377 München, Germany*

Erik A. Flügel

Erik A. Flügel was born in 1985 in Munich, Germany. He received his MSc in Chemistry at the Ludwig-Maximilians-Universität München (LMU) in 2011 and is currently doing his PhD under the supervision of Bettina V. Lotsch at LMU Munich. His research is focused on the synthesis of hierarchically structured MOFs.

Annekathrin Ranft

Annekathrin Ranft was born in 1985 in Munich, Germany. She received her MSc in Chemistry at LMU München in 2011. She is currently doing her PhD under the supervision of Bettina V. Lotsch on the fabrication of nanoscale MOFs and their integration in MOF-based optical sensors within the framework of the priority program 1362 "Porous Metal–Organic Frameworks" of the German Research Foundation.

modular and highly rational approaches to sophisticated network topologies, which is rarely seen in the synthesis of dense solid-state materials at elevated temperatures under thermodynamic control. The importance of the concepts "surface" and "porosity" associated with MOFs, together with their inherent functionality hosted by both organic and inorganic building blocks, gives rise to a kaleidoscope of properties and, hence, applications. The more traditional ones like adsorption,[4–6] gas storage[7,8] and separation[4,9,10] have been complemented in recent years by a host of emerging applications such as in sensor design,[5,11–13] light harvesting,[14,15] bioimaging,[16,17] drug delivery,[18–20] and catalysis.[21–24]

Such applications have been propelled by the ongoing downsizing of MOFs to the nanoscale and the prospect of amplifying large internal surface areas by ever increasing external surface areas and of combining inherent functionality with high sensitivity. The miniaturization of MOFs has already become one of the most prosperous disciplines in current MOF chemistry as it bridges the gap between fundamental MOF science and prospective applications by imprinting MOFs with morphologies suitable for device fabrication.

Nanosized MOF architectures (nanoMOFs), featuring at least one dimension at the nanoscale, offer significantly altered properties and reactivity compared to the bulk material. Increased textural porosity and external surfaces remove or diminish the mass transfer limits[25] and therefore increase the activity of catalysts as well as the response time in sensor applications. Additionally, materials with structures matching visible light wavelengths may exhibit optical effects based on interference and diffraction.[26] In biological applications, the internalization kinetics as well as blood half-life and the distribution of the particles throughout the biosystem have been found to be size-dependent.[27] For example, smaller particles have been shown to exhibit increased plasma circulation times and can even be transported to the lymphatic system.[28]

The exploration of synthesis strategies toward nanoMOFs and the exploitation of their small size constitute a nascent field that has materialized already in promising studies on the use of nanoMOFs, for example in medical applications. However, apart from size effects, the shape and morphology of nanoMOFs play a key role and are inherently relevant to the type of application that is sought. As R. E. Morris states, "A burgeoning challenge in the field is therefore to prepare the materials with shapes tailored for specific purposes, for example as thin films for membrane applications."[29] While spherical shapes ensure uniform framework degradation and hence, drug release, non-spherical or anisotropic shapes may be preferred in catalysis or optics due to the prominence of active sites at edges and corners or preferred orientation of channel systems. In contrast, MOF membranes or films exhibit suitable morphologies for gas separation or planar sensing platforms in devices such as vapor sensitive thin films[26] or quartz crystal microbalance-based sensing systems.[11,30] Taken together, the specific size, shape and morphology imbue nanoMOFs with functionality and reactivity that can be tuned in a large range depending on the finesse of the fabrication procedures.

This feature article is geared towards recent advances in MOF nanoscale synthesis and nanofabrication that have set the stage for the rational design of MOF nanomorphologies ranging from zero-dimensional (0D) and one-dimensional (1D) to two-dimensional (2D) and other anisotropic and hybrid nanostructures. The article is designed to focus on benchmark studies rather than to give a comprehensive account of the rapidly evolving nanoMOF field, and as such, we will highlight selected examples that have paved the way toward a better understanding of nucleation and growth at the nanoscale, or which are trend-setting with respect to novel strategies in nanoscale MOF synthesis.

For a more comprehensive overview of emerging applications of MOF nanomorphologies, the reader is referred to a number of

Frederik Haase

Frederik Haase was born in 1988 in Gießen, Germany. He received his Bachelor of Science in Chemistry and Biochemistry in 2011 at the LMU München. Currently he is pursuing his Master degree in Chemistry in the group of Prof. B. V. Lotsch. His research interest is focused on the development of novel strategies for the synthesis of nanoscale metal–organic frameworks.

Bettina V. Lotsch

Bettina V. Lotsch studied chemistry at the LMU München and the University of Oxford and received her PhD from LMU Munich in 2006. From 2007 to 2008 she joined the group of G. Ozin at the University of Toronto as a Feodor-Lynen postdoctoral fellow supported by the Alexander von Humboldt foundation. In 2009, Bettina Lotsch was appointed associate professor at LMU Munich, Germany, and since 2011 she has additionally held a group leader position at the Max Planck Institute for Solid State Research in Stuttgart. Her research interests include multifunctional and hierarchically porous framework materials, "smart" photonic crystals, as well as two-dimensional materials for energy conversion and storage.

excellent reviews that have recently appeared on this topic, such as those by Lin,[19] Spokoyny,[31] or Shekhah.[32]

2. Zero-dimensional nanostructures

2.1 Sonochemical and microwave-assisted syntheses

The synthesis of zero-dimensional MOF nanoparticles has been achieved by a number of protocols so far, which mainly rely on the spatial and temporal control of nucleation and growth of MOF crystals under solvo- or hydrothermal conditions. Along these lines, the concept of arrested particle growth has been implemented successfully by adding so-called coordination modulators, *i.e.* inhibitors such as monocarboxylic acids,[33,34] or by the *in situ* activation of ligands as realized in the deprotonation of 2-methylimidazole to speed up ZIF-8 nucleation.[35,36] In general, the most convenient protocols for nanoMOF synthesis are those that require minimum *chemical* reaction control (addition of modifiers, surfactants, reactant ratio), but solely rely on growth control *via physical* parameters, such as the type of energy supply, reaction time and temperature. Therefore, a number of methodologies have been developed recently, exploiting either conventional electric (CE),[37] ultrasonic (US)[38,39] or microwave (MW) assisted heating[40,41] for the synthesis of nanoMOFs. The use of US irradiation in the synthesis of nanosized MOFs was first adapted from organic synthesis by Qiu *et al.*, who were able to synthesize a fluorescent microporous nanoMOF $[Zn_3(btc)_2 \cdot 12H_2O]$ (*btc* = 1,3,5-benzenetricarboxylate) by using US treatment at room temperature[38] and has since then been successfully extended to various other systems like ZIF-8 and HKUST-1.[42] US effects originate from acoustic cavitation, which generate local hot spots with high transient temperature (5000 K), high pressure (>1000 atm), and rapid heating and cooling rates (10^{10} K s^{-1}).[43,44] The nucleation and growth of the particles preferably take place at these hot spots, which limits the particle size as the spots cool down to the temperature of the reaction medium within milliseconds.

MW-assisted synthesis has turned out to be another promising technique to achieve the formation of MOF nanoparticles. The method initially relied on a droplet liquid dispersion protocol taking advantage of the rapid evaporation of a reactant-containing organic solvent mixed with water by MW heating.[45,46] However, this method can be transferred to homogeneous solvent systems by taking advantage of the high dielectric absorptivity of polar solvents such as diethylformamide (DEF), which leads to rapid thermal energy conversion and efficient local heating of the reaction solution, thereby affording fast nucleation and crystal growth. Along these lines, Ni *et al.* reported the first successful synthesis of IRMOF-1, -2, and -3 nanoparticles by the so-called MW-assisted solvothermal synthesis, which has since then been picked up successfully by others to efficiently and size-selectively synthesize various MOF nanoparticles.[41,47–49]

Both sonochemical and microwave syntheses have been found to significantly accelerate MOF crystallization as compared to traditional electric heating, while the observed rate enhancement is typically larger for US than MW irradiation. Recent work has shown that both the rates of nucleation and crystal growth are greatly enhanced by US and MW irradiation compared to classical solvo-/hydrothermal syntheses, which is attributed to increased pre-exponential factors of the Arrhenius equation and hence, increased reaction probability (Fig. 1).[47]

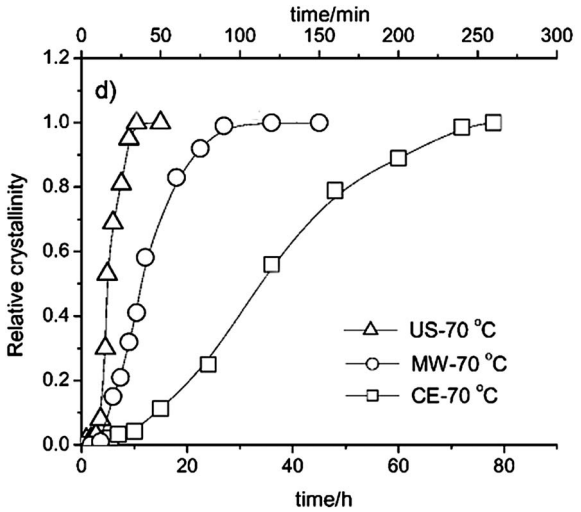

Fig. 1 Increase in crystallinity of MIL-53 (Fe) with time compared for US, MW and CE heating. Reproduced with permission from ref. 47. Copyright© 2011 by John Wiley & Sons, Inc.

It needs to be pointed out, however, that for different MOF systems different relative accelerations of nucleation and crystal growth, respectively, are observed. The impact of nucleation rate enhancement was found to be dominant in systems such as $Cu_3(btc)_2$,[50] while acceleration of crystal growth is more important in MIL-53(Fe).[47] Taking into account the reaction yield and monodispersity of the resulting nanoparticles, which are key factors from a preparative point of view, Chalati *et al.* have found that for MIL-88A MW-assisted synthesis is superior to both conventional hydrothermal and US synthesis. Whilst both US and MW syntheses excel with respect to the rapid formation of nanoparticles smaller than 100 nm, US-assisted protocols require highly dilute solutions and the additional use of coordination inhibitors such as acetic acid, resulting in very small yields (<10%). In contrast, MW-assisted synthesis affords MIL-88A nanoparticles with good size control, being almost unaffected by the concentration (up to 1 mmol L^{-1}), and a relatively high yield independent of the reaction time.[51]

2.2 Microemulsion synthesis

Besides size control by different types of energy transduction, zero-dimensional MOF nanoparticles have been synthesized by taking advantage of interfacial reactions providing shape control and confinement of the reaction zone at the same time. For example, a highly attractive route to MOF nanospheres has recently been reported by Zhao *et al.*, who used surfactants to limit the size of the resulting particles and as a template to create micro–mesoporous MOF structures at the same time.[52] Highly ordered hierarchically porous structures were obtained by combining the solvating possibilities offered by ionic liquids (ILs) and supercritical CO_2 ($SCCO_2$) with the templating properties of fluorocarbon-type surfactants. The surfactant *N*-ethyl perfluorooctylsulfonamide (*N*-EtFOSA) forms microemulsions

in a solvent mixture of the IL 1,1,3,3-tetramethylguanidinium acetate (TMGA) and $SCCO_2$, as the interactions between CO_2 and the fluorocarbon tails of the surfactants are strong.[53,54] In a standard synthesis procedure, $Zn(NO_3)_2$, 1,4-benzenedicarboxylic acid (H_2bdc) and *N*-EtFOSA were added to TMGA and heated in a high-pressure cell under 16.8 MPa CO_2 pressure at 80 °C for 48 h. Transmission electron microscopy (TEM) images (Fig. 2) show nanoparticles of roughly 80 nm diameter with a uniform size distribution and a well ordered system of mesopores. The pore size was found to be 3.0 nm, whereas the microporous pore walls have a thickness of 2.5 nm. Although the structure of the pore walls could not be identified by comparison with known Zn(*bdc*)-type MOF structures, N_2-sorption measurements reveal well-pronounced mesoporosity along with moderate microporosity and a bimodal pore size distribution centered at 3.6 nm and 0.7 nm.

2.3 Interfacial synthesis

A very elegant realization of interfacial control has been put forward by De Voss and co-workers, who demonstrated the fabrication of hollow MOF capsules at the interface between two immiscible liquids.[55] The inorganic (copper acetate) and organic (H_2btc) precursors were separately dissolved in water and 1-octanol, respectively, and both liquids were supplied by syringe pumps to a T-junction, where water droplets were generated by breaking-off in the co-flowing organic ligand solution as demonstrated in Fig. 3. The obtained micron-sized capsules (~375 μm) feature defect-free walls of about 2 μm thickness due to a self-completing growth mechanism, which has nicely been demonstrated by the efficient retention of encapsulated Rose Bengal dyes within the intact walls of the MOF capsules.

While the thickness of the walls is clearly above the nanometre range, the interfacial formation of nanoscale MOF membranes based on this biphasic synthesis approach is clearly within reach. Moreover, the tuning of solvents, MOF precursors, concentrations and flow rates will further broaden the scope of this methodology and bodes well for the fabrication of freestanding MOF films as well as versatile MOF nanocontainers with microporous walls and, hence, size-selective storage and release properties. This could lead to future applications in catalysis by trapping molecular catalysts inside MOF capsules to form micro- or even nanoreactors. An overview of all presented synthesis strategies discussed in this chapter is provided in Table 1.

3. One-dimensional nanostructures

3.1 Surfactant-assisted synthesis in reverse microemulsions

While the synthesis of MOF nanoparticles has been rather widely explored, the search for a generalized approach to the synthesis of anisotropic and especially one-dimensional nanostructures such as wires and rods has received less attention. Nevertheless, progress has been made with respect to interfacial synthesis procedures in heterogeneous phase mixtures. Among these approaches, surfactant-assisted syntheses in reverse microemulsion systems have shown potential in controlling the shape and aspect ratio of nanoMOFs, although the direct correlation between emulsion composition and the resulting shapes is elusive in most cases.

Lin and co-workers developed a synthetic strategy utilizing the size limiting effects of reverse microemulsions to synthesize MOF nanostructures.[63–65] Both shape and size of the micelles can be altered by adjusting the surfactant to water ratio ω, resulting in surfactant-stabilized water reservoirs in a continuous organic phase, which can be used as nanoreactors for MOF synthesis. The authors prepared $Ln(bdc)_{1.5}(H_2O)_2$ (Ln = Eu^{3+}, Gd^{3+} or Tb^{3+}) in a microemulsion system consisting of the cationic surfactant cetyltrimethylammonium bromide (CTAB), isooctane, 1-hexanol and water, using $LnCl_3$ and dimethylammonium-1,4-dicarboxylate as MOF precursors. By varying the

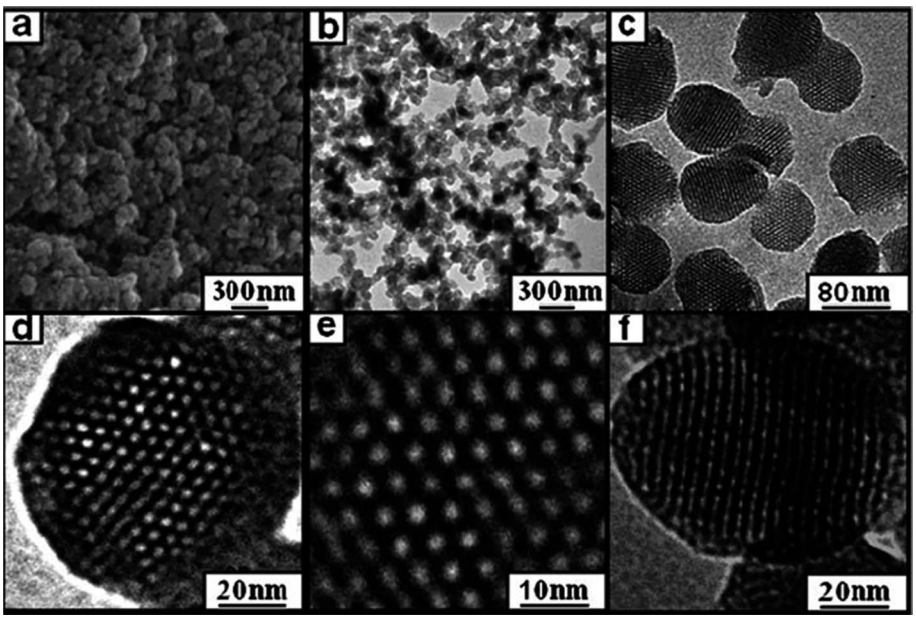

Fig. 2 (a) Scanning electron microscopy (SEM) and (b–f) TEM images of hierarchically micro- and mesoporous MOF nanoparticles. Reprinted with permission from ref. 52. Copyright© 2011 by John Wiley & Sons, Inc.

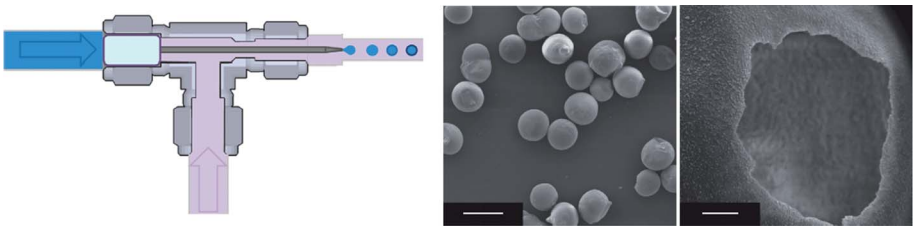

Fig. 3 Left: cut-away view of the T-junction showing details of the emulsification step. The metal-ion containing aqueous phase (blue) flows through a tapered capillary in the tubing, and the ligand-containing organic solution (purple) flows around it. Growing droplets detach when the force due to interfacial tension is exceeded by the drag force of the surrounding organic phase. Middle: SEM micrograph showing several capsules and their monodispersity. Scale bar 500 μm. Right: SEM micrograph of a capsule crushed with a needle tip showing its hollow interior. Scale bar 25 μm. Reprinted with permission from ref. 55. Copyright© 2011 by Nature Publishing Group.

Table 1 Overview of various synthesis approaches towards 0D nanostructures and the resulting morphology and sorption properties of the formed particles in comparison to the respective bulk material

0D nanostructures				Bulk
Synthesis method	References	Selected examples	Properties	Properties
Coordination modulation	33,35,36,40 and 56–58	ZIF-8	9 nm (Ø), rhombic dodecahedra, 1617 $m^2 g^{-1}$ (for 18 nm sized particles) (ref. 35)	Micrometre sized rhombic dodecahedra, 1630 $m^2 g^{-1}$ (ref. 59)
Ultrasonic synthesis	36,42 and 47	HKUST-1	10 nm (Ø), spherical particles, 1075 $m^2 g^{-1}$ (ref. 42)	Micrometre sized octahedra, 2260 $m^2 g^{-1}$ (ref. 60)
Microwave	34,39,41,46 and 47	IRMOF-3	(Sub)micrometre sized cubic crystals[a] (ref. 41)	Micrometre sized cubes, 2160 $m^2 g^{-1}$ (ref. 61)
Interfacial synthesis	55	HKUST-1	375 μm (Ø), hollow capsules, 620 $m^2 g^{-1}$ (ref. 55)	Micrometre sized octahedra, 2260 $m^2 g^{-1}$ (ref. 60)
Ionic liquids/ microemulsion	22	$Gd_2(bdc)_3(H_2O)_4$	100 nm (Ø) × 35 nm, irregularly shaped platelets[a] (ref. 22)	Blade-like crystals, no sorption observed for N_2(g) and CO_2(g) (ref. 62)

[a] No sorption data available.

ω-value from 5 to 10, the aspect ratio of the resulting MOF nanorods could be altered from 100–125 nm length and 40 nm diameter (ω = 5) up to 2 μm length and a diameter of 100 nm (ω = 10). While increasing the concentration does not affect the aspect ratio of the nanocrystals, it decreases the particle size, possibly due to the increased number of nucleation sites present in the higher concentrated synthesis solution. Additionally, the presence of the surfactant, which creates a shell-like structure around the growing particles, seems to enhance the stability of the particles against agglomeration.[19] These nanoMOFs could lead to applications in bioimaging due to the high concentration of highly paramagnetic metal ions such as Gd^{3+}, which are administered to enhance magnetic resonance image contrast by increasing proton relaxation rates.[63]

The above synthesis scheme was extended to MOFs with higher biocompatibility, while retaining MRI contrast enhancing properties, by the synthesis of Mn^{2+}-based MOFs with *bdc* and *btc* linkers. The resulting rod-shaped nanoMOFs of $Mn(bdc)(H_2O)_2$ crystallize in the bulk crystal structure and feature tuneable aspect ratios with lengths up to several microns. In contrast, nanoMOFs of composition $Mn_2(btc)_3(H_2O)_6$ exhibit an unusual spiral rod morphology with a crystal structure not corresponding to previously known Mn^{2+}-*btc*-based phases (Fig. 4).[65]

3.2 Interfacial control in a microfluidic environment

In recent years, "Lab-on-a-Chip" devices for the synthesis of 1D-nanostructures have entered the focus of synthetic chemists.[66–68] An elegant method for the preparation of 1D nanowires of coordination polymers that exploits interfacial chemistry in a microfluidic environment has recently been presented by Dittrich and co-workers.[69] The reactant solutions are injected parallel into a microfluidic chip creating a laminar flow of the reactant solutions, thereby enabling superior control of the interface region acting as a reaction zone.

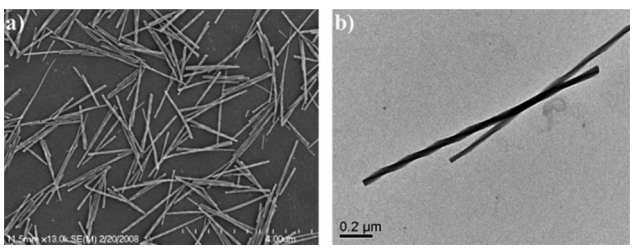

Fig. 4 (a) SEM and (b) TEM images of $Mn_3(btc)_2(H_2O)_6$ spiral nanorods synthesized at room temperature. Reprinted with permission from ref. 65. Copyright© 2008 American Chemical Society.

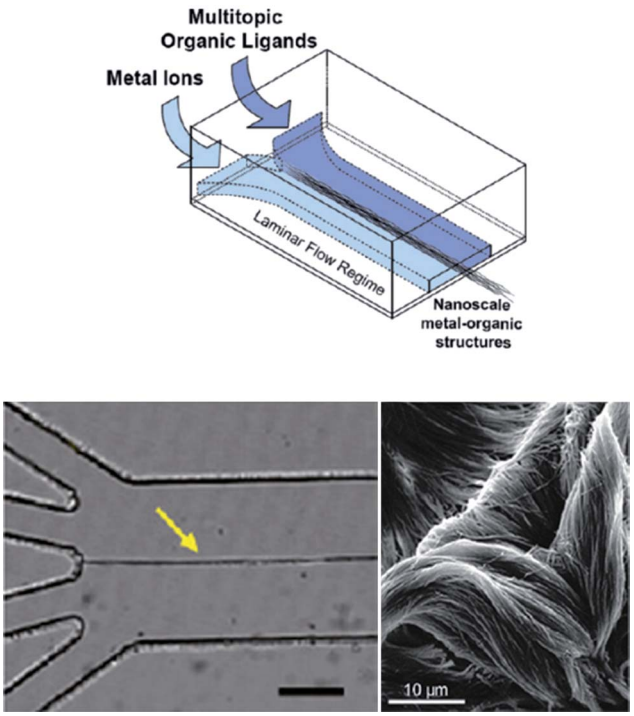

Fig. 5 Top: schematic drawing of the laminar flow of the reactants in a microfluidic device. Bottom left: microscopic image of the formed nanowires at the interface between both reactant flows; bottom right: SEM image of a bundle of Cu(II)-Asp nanowires. Reprinted with permission from ref. 69. Copyright© 2011 American Chemical Society.

In Dittrich's setup, two aqueous solutions of $Cu(NO_3)_2$ and L-aspartate (Asp) in NaOH were injected into a microfluidic device with four input channels at a flow rate of 100 μL min^{-1}. At the interface of both streams, nanowires formed within microseconds, which were identified as Cu(II)-Asp by XRD analysis. Scanning electron microscopy (SEM) measurements proved the formation of bundles of well-aligned nanowires (Fig. 5).

The scope of this synthesis scheme has been extended to nanofibers of Ag(I)-cysteine (Cys) and Zn(II)-4,4′-bipyridine (4,4′-bipy) coordination polymers with rather uniform diameters in the sub-100 nm range. Although this intriguingly simple microfluidic scheme has not yet been used to produce porous MOF nanowires, it can in principle be utilized to fabricate a wide range of different 1D MOF nanostructures. A major drawback, however, is the lack of scalability, rendering this technique in its present form unsuitable for preparative chemistry and industrial production schemes.

3.3 Coordination modulators

Capping agents have proven valuable in restricting particle growth by reacting with the surface of the particles and preventing further molecular addition from the mother liquor. Suitable capping agents, among others, are molecules having a single functionality able to form a bond with the metal ions of the metal–organic framework, termed monolinkers. The possibility to terminate the growth of nanoparticles by coordination modulation has been successfully demonstrated by Kitagawa and co-workers using $[Cu_3(btc)_2]$ as a model system.[40] Notably, the addition of such growth inhibitors may permit valuable insights into MOF growth and can even be used to modulate the shape of nanosized MOFs.

Along these lines, Tsuruoka *et al.* have shown that the addition of monolinkers with a functionality identical to that of the framework constituents can yield crystals with anisotropic shapes (Fig. 6).[33] In the three-dimensional layer-pillar-type framework $[Cu_2(ndc)_2(dabco)_n]$ (*ndc* = 1,4-naphthalene dicarboxylate; *dabco* = 1,4-diazabicyclo[2.2.2]octane), the *ndc*-linkers connect the copper clusters in the [100] and [010] directions, while *dabco* connects the clusters in the [001] direction of the crystal. This inherent framework anisotropy based on two different coordination modes (copper–*ndc* and copper–*dabco*), which is imprinted in the tetragonal crystal structure, can be exploited to create different dimensionalities of the formed crystals. By adding a monocarboxylic acid such as acetic acid to the reaction mixture, further addition of *ndc* to the network is inhibited, leading to the formation of square-rod shaped nanocrystals with average lengths of 392 ± 210 nm and thicknesses of 82 ± 23 nm, respectively. The major axis of the nanorod was found to be coincident with the [001] direction of the framework, indicating preferred crystal growth along the copper–*dabco* interactions. The addition of a competitive linker to *dabco* should hence lead to the formation of nanosheets, but this hypothesis is yet to be proven. Interestingly, by studying the time evolution of the reaction by TEM, the growth mechanism was found to proceed by oriented attachment of medium-sized nanocubes (80 nm), as evidenced by the constant diameter of the formed nanorods of roughly 80 nm and the stepwise increase of the aspect ratio. This

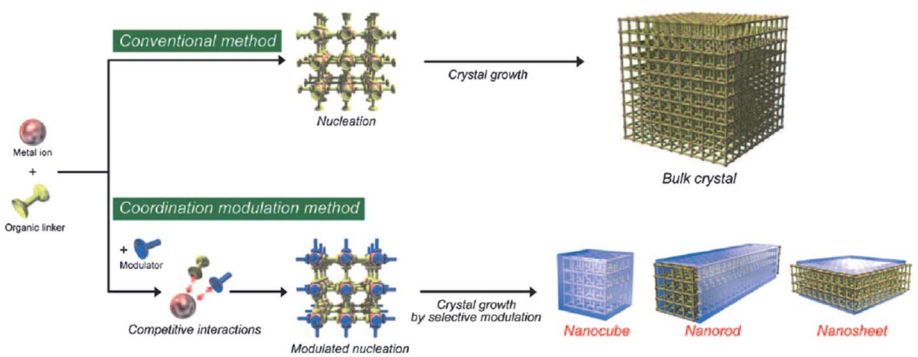

Fig. 6 Conventional synthesis of metal–organic frameworks contrasted with the coordination modulation method to produce anisotropic nanostructures. Reprinted with permission from ref. 33. Copyright© 2009 by John Wiley & Sons, Inc.

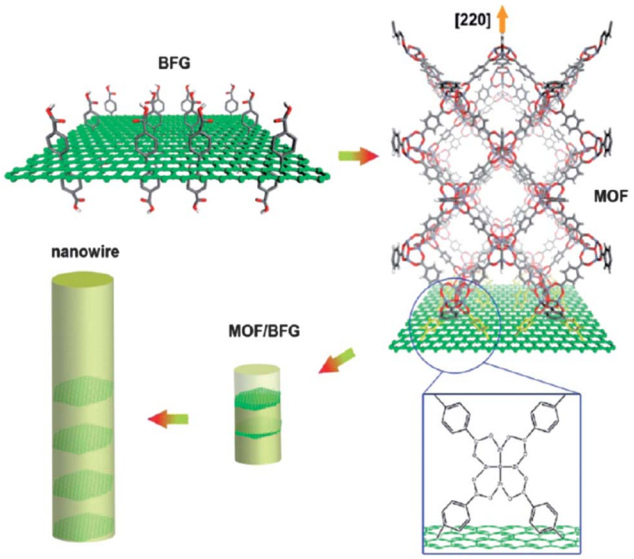

Fig. 7 Schematic of the proposed bonding between BFG and MOF *via* COOH groups along the [220] direction, and the proposed assembly into nanowire structures with incorporated BFG. Reprinted with permission from ref. 71. Copyright© 2010 American Chemical Society.

is, perhaps not too surprisingly, the first strong evidence that the classical oriented attachment growth model familiar from a range of other nanomaterials[70] likewise can occur in MOF systems.

3.4 Growth templates

An intriguing, yet unusual approach to grow MOF nanowires utilizes appropriately functionalized surfaces akin to SURMOFs grown from suitable organically modified substrates (see Section 4.3). Recently, Jahan *et al.* elegantly transferred this concept to "freestanding surfaces", *i.e.* to the use of chemically modified graphene nanosheets acting as nucleation sites for MOF-5 nanocrystals.[71] Firstly, by modifying reduced graphene oxide (GO) sheets with benzoic acid, carboxylic acid groups were introduced on both sides of the graphene sheets. The so-called BFG (benzoic acid functionalized graphene) was then mixed with 1,4-*bdc* and $Zn(NO_3)_2$, forming a hybrid material consisting of MOF-5 and BFG sheets. Notably, at 5 wt% BFG a clear transformation into nanowire morphology was observed, which was accompanied by profound changes in the MOF crystal structure. Interestingly, the attachment of BFG to the tip of the resulting nanowires along with its integration into the body of the wire as evidenced by micro-Raman analysis attests to a dual interaction between BFG and MOF and, hence, points to the following growth mechanism (Fig. 7): on the one hand, the average diameter of the graphene sheets amounts to roughly 300 nm, which coincides well with the diameter of the MOF nanowires. Hence, BFG acts as a nucleation template, providing a high density of carboxylic acid anchoring sites. On the other hand, TEM analyses reveal that the wires grow along the [220] direction with their (220) faces exposed. These facets incidentally exhibit the highest concentration of Zn_4O clusters, thus resulting in strong metal–carboxylate binding interactions favoring growth in this particular direction as well as the integration of BFG into the body of the growing MOF nanowire. Even if this discovery may have been driven by serendipity, it is trendsetting in revealing the potential of template-directed heterogeneous nucleation and growth for the design of anisotropic MOF nanostructures. An overview of all presented synthesis strategies discussed in this chapter is provided in Table 2.

4. Two-dimensional nanostructures

The fabrication of 2D-MOF nanostructures, *i.e.* thin films and membranes tailored to the need of specific applications, has dramatically picked up pace in recent years. This is because a number of complementary growth schemes has been devised that each address and imply different morphologies and substrate requirements. So far, MOF thin films have been obtained by six different synthetic schemes, including (a) direct oriented or non-oriented growth from preconditioned solvothermal mother liquors,[9,74–77] (b) electrochemical growth of MOF films on suitable metal substrates, including Galvanic displacement,[78] (c) deposition from colloidal MOF suspensions,[6,34] (d) deposition of MOF films based on a gel-layer approach,[79–81] (e) stepwise growth of thin MOF films utilizing a layer-by-layer (LbL) methodology,[82–87] and (f) top-down

Table 2 Overview of the synthesis approaches towards 1D nanostructures and the resulting morphology and sorption properties of the formed structures in comparison to the respective bulk material

1D nanostructures				Bulk
Synthesis method	References	Selected examples	Properties	Properties
Coordination modulation	33	$Cu_2(ndc)_2(dabco)_n$	392 nm × 82 nm rods[a] (ref. 33)	Microcrystalline powder, 1891 $m^2\ g^{-1}$ (ref. 72)
Surfactant-assisted synthesis/ reverse microemulsion	22,52,64 and 65	$Gd_2(bdc)_3(H_2O)_4$	125 nm × 40 nm rods[a] (ref. 22)	Blade-like crystals, no sorption observed for N_2(g) and CO_2(g) (ref. 62)
Interfacial synthesis/ microfluidics	69	Zn(II)-4,4′-bipyridine	10–75 nm (Ø) fiber bundles[a] (ref. 69)	Micrometre sized needle-like crystals[a] (ref. 69)
Templating	71	MOF-5	300 nm (Ø) wires, 809 $m^2\ g^{-1}$ (ref. 71)	Millimetre sized cubes, 2900 $m^2\ g^{-1}$ (ref. 73)

[a] No sorption data available.

fabrication of freestanding, atomically thin MOF layers.[88] As a number of comprehensive reviews surveying each of the above growth methods exists,[32,57,89] we will focus our attention to those schemes that furnish nanoscale thin films (primarily methods (c), (d), (e) and (f)), rather than micron-scale layers typically obtained by methods (a) and (b).

4.1 Deposition of MOF colloids

Though being a rather recent approach, the deposition of MOF thin films from colloidal suspensions is one of the key methods for film fabrication owing to its simplicity and facile production of films with high optical quality on various substrates. Horcajada *et al.* reported on the fabrication of thin films processed by dip-coating of an iron muconate (MIL-89) colloidal sol containing nanoparticles between 20 and 40 nm in size.[34] The optical quality of the resulting films allowed *in situ* characterization by environmental ellipsometry, demonstrating the reversible increase in cell volume of the highly flexible MOF by adsorption of polar liquids and the resulting decrease in the refractive index of the layer from 1.65 to 1.45 upon swelling. Similar films have been produced based on MIL-101 (Cr) and other MOFs, featuring layer thicknesses typically below 80 nm, which could be increased by multiple dipping steps (Fig. 8).[90]

Owing to the deposition from colloidal suspensions, the films feature bimodal porosities resulting from both structural and textural porosity, the latter being introduced by inter-grain voids typically in the mesopore range. Hierarchical micro- and mesoporosity may turn out beneficial in applications where fast diffusion into the MOF micropores through mesoporous interparticle voids is key, such as in catalysis or size-selective adsorption from vapor mixtures. This increased sensitivity to guest molecules can be used to enhance MOF-based Fabry–Pérot sensor devices, which have already been synthesized *via* direct growth.[26] Another advantage of the colloidal deposition method, which can easily be extended to spin- or spray-coating protocols, lies in its indiscriminate nature with respect to substrate requirements, as no surface modification prior to the coating step is necessary.

4.2 Gel-layer approach

Colloidal deposition routes result in random orientation of the nanoparticles on the surface, hence not allowing for oriented MOF growth along specific crystallographic directions. In contrast, oriented MOF growth has been observed in the gel-layer approach developed by Bein and co-workers,[80] and is inherent to the LbL protocol that has been pioneered by the groups of Wöll and Fischer.[81] In the novel gel-layer approach, a gold substrate primed by self-assembled monolayers (SAMs) as nucleation-directing templates[79] is loaded with the metal-salt-containing poly(ethyleneglycol) gel layer and subsequently covered with a solution containing the linker molecules. Highly oriented and uniform submicron thick layers have successfully been grown with HKUST-1 and the flexible framework Fe-MIL-88B_NH_2 within reaction times of typically two days. As the layer thickness is tunable by adjusting the metal ion concentration in the gel layer, this approach represents a simple, yet highly efficient approach toward oriented MOF films with variable thicknesses. Although highly oriented films have also been grown from preconditioned mother solutions in a direct fashion,[75] the gel approach allows for a more subtle control of the growth zone and hence layer thickness.

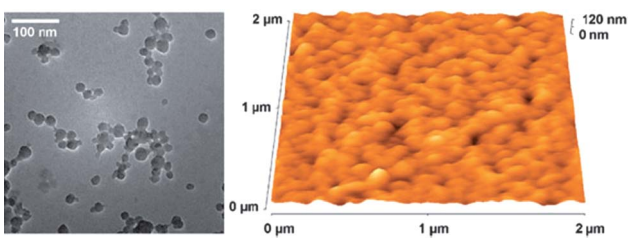

Fig. 8 TEM (left) and atomic force microscopy (right) images of nanoparticles and a thin film of MIL-101 (Cr) made by nanoparticle deposition, respectively.[90] Reproduced by permission of The Royal Society of Chemistry.

4.3 Layer-by-layer growth (liquid phase epitaxy)

The technology of MOF thin film synthesis affording the highest level of control in terms of composition, crystallographic orientation and structure, thickness and even post-modification by selective pore loading, relies on the stepwise LbL growth christened "liquid phase epitaxy" (LPE) owing to the unique orientation control possible with this technique.

The stepwise growth of surface immobilized MOFs (dubbed SURMOFs) was first introduced by Shekhah *et al.* in 2007, who were able to demonstrate the feasibility of controlling not only the orientation, but also the number of MOF layers grown on the surface.[81] Instead of the single-pot solvothermal synthesis used

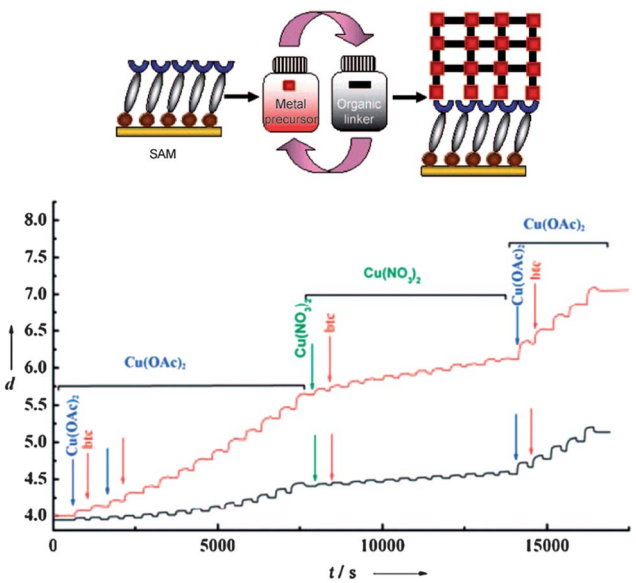

Fig. 9 Top: generalized scheme of a LbL synthesis of MOF thin films on SAM terminated surfaces. Bottom: SPR signal as a function of time recorded *in situ* during the stepwise treatment of two different SAMs (11-mercaptoundecanol (MUD) in red, 16-mercaptohexadecanoic acid (MHDA) in black) with $Cu(OAc)_2$, H_3btc, and $Cu(NO_3)_2$. Reprinted with permission from ref. 87. Copyright© 2009 by John Wiley & Sons, Inc.

by Fischer and Bein,[80,81] HKUST-1 was grown in a LbL fashion by repeated immersion cycles using two precursor solutions, each containing one reactant (Fig. 9). As with each immersion cycle another layer is added to the structure, the thickness of the resulting MOF film can be controlled by limiting the number of immersion cycles. Intriguingly, each immersion cycle can directly be observed *in situ via* quartz crystal microbalance analysis by monitoring the change in resonance frequency, or by surface plasmon resonance spectroscopy,[87] demonstrating the precise growth of the film with sub-monolayer resolution.

The effect of different SAMs on the orientation of the MOF layers has been demonstrated by Shekhah *et al.* who studied the influence of COOH- and OH-terminated SAMs on the orientation of HKUST-1.[87] By functionalizing gold substrates with those SAMs, it could be shown by out-of-plane XRD measurements that COOH terminated surfaces lead to (100) oriented HKUST-1 films by strong interactions between exposed Cu_2 dimeric units and the carboxylic acid termini, while OH-groups provide a better surface for (111) orientation owing to beneficial Cu^{2+}–OH interactions.

Recently, the same groups proposed a new and faster synthesis route towards MOF thin films using a modified layer-by-layer approach. In contrast to previous LPE procedures, the reactants were now deposited *via* spray-coating on a surface modified with SAMs, thereby allowing for a significantly faster deposition speed as well as the fabrication of micron thick monolithic films. Washing steps between the sequential spray-coating of the individual reactant solutions have turned out to be crucial as they ensure that no additional substructures can be formed from excess reactants and the subsequently deposited reactant solution. Nevertheless, a substantially increased SURMOF thickness per deposition cycle is observed with spray coating as compared to the traditional LPE method, which is likely due to incomplete reactant removal by the washing steps. Though being beneficial for rapid film growth (20 full cycles afford 200 nm film thickness in 30 min), these observations render the exact growth mode in the spray process still subject to debate.[84]

The LPE surface growth of MOFs transcends classical LbL schemes introduced by Decher and others for oppositely charged polyelectrolytes[83] in that it furnishes crystalline order both perpendicular and parallel to the substrate, combined with an exceptionally high level of compositional control at the atomic scale. It should be noted, however, that these achievements are intrinsically connected with the use of high quality SAM-modified substrates, as the crystalline order of the particular SAM chosen will be directly imprinted into the MOF film grown on top. Furthermore, it remains to be shown that the LPE scheme can be generalized to MOF compositions other than the typically used HKUST-1 and layer-pillar MOFs. An important step in this direction has recently been taken by the selective growth of a so far unknown, non-interpenetrated MOF-508 structure based on Zn^{2+}, *bdc* and 4,4′-bipyridine building blocks by the LPE approach.[82] The formation of the interpenetrated bulk structure is likely suppressed by the presence of the substrate, thus lifting the equivalence of the otherwise identical sublattices. This result bodes well for a more generalized approach toward surface-induced formation of new framework topologies *via* the LPE method.

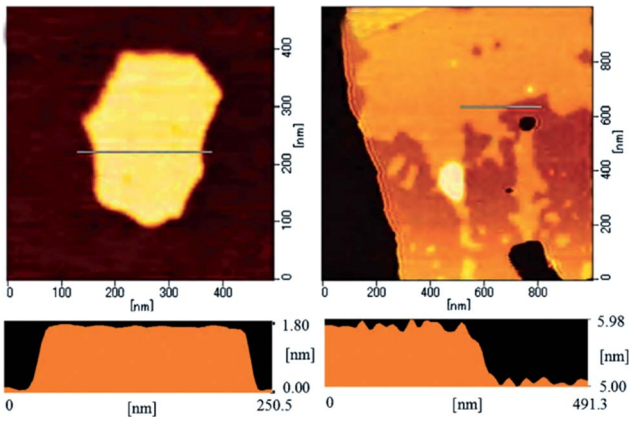

Fig. 10 Tapping-mode AFM images of delaminated MOF-2 nanosheets deposited on a mica substrate showing (left) a MOF-2 nanosheet with the thickness of ~1.5 nm and (right) a profile of two neighbouring overlapped layers of delaminated MOF-2 nanosheets with a distance of ~0.7 nm between both layers.[88] Reproduced by permission of The Royal Society of Chemistry.

4.4 Top-down fabrication

The final and most recent fabrication method for MOF thin films may be considered as a "top-down" or "deconstruction" method starting out from a bulk MOF material. Li *et al.* produced atomically thin MOF layers by delamination of a dried sample of bulk MOF-2 by ultrasonication in acetone.[88] MOF-2, a 2D network constructed by paddle-wheel Zn_2-clusters and terephthalates held together by hydrogen bonds,[91] lends itself ideally as a model system for exfoliation studies owing to its weak interlayer forces. The as-produced nanosheets were shown by AFM to have thicknesses between 0.7 and 6.0 nm and lateral dimensions between 100 nm and 1 μm (Fig. 10), corresponding well to the theoretical thickness of a single MOF-2 sheet (0.75 nm). Restacking in the presence of amines led to intercalated aggregates with increased layer spacings, yet more quantitative data will be needed in order to gauge the adsorption/intercalation capacities of MOF nanosheets and potential applications as sorption and storage media. An overview of all presented synthesis strategies discussed in this chapter is provided in Table 3.

5. Hybrid nanomorphologies

While shape already imparts functionality to MOF nanocrystals, the level of functionality can significantly be raised by tuning the composition or by integrating different properties within one single MOF platform. This may be done by various schemes, the most prominent being post-synthetic modification (PSM) of the linkers in as-obtained frameworks and the surface-modification of as-formed MOF nanoparticles. The former synthesis strategy can be used for materials having functional groups attached to the linker molecules, which can be modified with the desired reactant in the functionalization step. As a requirement, the frameworks must be stable under functionalization conditions as well as to by-products formed during the functionalization process. In contrast to surface modification schemes, the framework must exhibit pores, being large enough for the

Table 3 Overview of the synthesis approaches towards 2D nanostructures and the resulting morphology and sorption properties of the formed layers in comparison to the respective bulk material

2D nanostructures				Bulk
Synthesis method	References	Selected examples	Properties	Properties
Coordination modulation	33	$Cu_2(ndc)_2(dabco)_n$	[a]	Microcrystalline powder, 1891 $m^2 g^{-1}$ (ref. 62)
Colloidal MOF-suspensions	34 and 90	MIL-101 (Cr)	22 nm spherical particles/48 nm thin film, 4200 $m^2 g^{-1}$ (ref. 90)	Microcrystalline powder, 5900 $m^2 g^{-1}$ (ref. 90)
Gel-layer deposition	74–77 and 79	HKUST-1	600 nm thin film (after 112 h)[a] (ref. 79)	Micrometre sized octahedra, 2260 $m^2 g^{-1}$ (ref. 60)
Layer-by-layer growth/liquid phase epitaxy	81 and 85–87	HKUST-1	200 nm thin films after 20 full cycles[a] (ref. 87)	Micrometre sized octahedra, 2260 $m^2 g^{-1}$ (ref. 60)
Top-down fabrication	88	MOF-2	200 nm × 300 nm × 1.5 nm sheets[a] (ref. 88)	Micrometre sized prisms, 270 $m^2 g^{-1}$ (ref. 73)

[a] No sorption data available.

reactants to enter in order to allow for a complete functionalization of the framework. The feasibility of PSM was already pointed out in 1990 by Hoskins *et al.*, who stated that "relatively unimpeded migration of the species throughout the lattice may allow chemical functionalization of the rods subsequent to the construction of the framework."[92] To date, a variety of possible PSM approaches have been explored, with the two main foci being on biomedical applications[93–95] and the exploration of otherwise inaccessible MOF compositions.[96] However, PSM on nanoMOFs is still a surprisingly scarce topic in state-of-the-art MOF science and, hence, we will turn our focus on surface-modification of nanoMOFs rather than PSM.

5.1 Core–shell particles

The groups of Férey and Lin have carried out pioneering works in the exploitation of biomedical applications based on surface-modified nanoMOFs, which have shown great potential for the encapsulation and controlled release of drugs.[97–99] In order to ensure maximum biocompatibility, optimal blood circulation times and release kinetics, as well as suitable administration of the drugs, MOFs have been coated by hydrophilic polymers such as poly(ethylene glycol) (PEG), or thin silica shells that can further be modified by grafting functional molecules on the exposed surface.[93,99]

For example, in a seminal study Férey and co-workers were able to prove the general concept of using nanosized MOF particles as efficient carriers for anti-cancer drugs. To this end, protocols for the synthesis of MIL-100 (Fe) nanoparticles *via* microwave synthesis were developed,[99] and the sub-200 nm particles were loaded with up to 25 wt% of busulfan, a commonly used anti-cancer drug. To enhance the stability of the MOF particles in biological systems, the authors coated the particles with bifunctional PEG (CH_3–O–PEG–NH_2, 5 mg per mL of water). Studies on human cell cultures showed that busulfan in nanosized MOFs and free busulfan exhibit the same activity, thereby paving the way for the use of suitably modified nanoMOFs as possible anti-cancer drug vehicles.

Lin and his group put forward studies on the biocompatibility of nanosized MOFs, thereby designing ways to enhance the stability of the particles inside biological systems.[95] By adding an ethanolic solution of tetraethylorthosilicate (TEOS) containing 4% aqueous ammonia to as-synthesized MIL-101 (Fe) nanoparticles, a silica shell is formed around the framework particles with thicknesses between 2 and 9 nm, depending on the reaction time (2–3 nm: 2 h, 8–9 nm: 7 h). As a consequence of the stabilizing shell, the half-life in phosphate buffered saline (PBS) solution at 37 °C is increased from 2.5 hours to 16 hours.

Furthermore, Lin and his group proved the possibility to functionalize nanoMIL-101 (Fe) particles (Fe^{2+} connected by NH_2-*bdc* and 1,4-benzenedicarboxylate linkers) with organic fluorophores such as 4,4-dibromo-4-bora-3*a*,4*a*-diaza-*s*-indacene (Br-BODIPY). This modification enables the use of the nanoparticles as imaging vehicles, using the fluorophore as a visible marker. The functionalisation with a prodrug of cisplatin (ethoxysuccinatocisplatin, ESCP) showed the possibility of using the particles also as drug carriers, as the cytotoxicity of the ESCP-functionalized particles on HT-29 human colon adenocarcinoma cells was comparable to other Pt drugs.[100] The combination of drug cytotoxicity with the increased biostability renders the nanoparticles capable of acting as targeted drug vectors with a controllable release rate due to the slow diffusion of metal and organic constituents through the silica shell, thus boding well for a new generation of "nanobioMOFs" (Fig. 11).

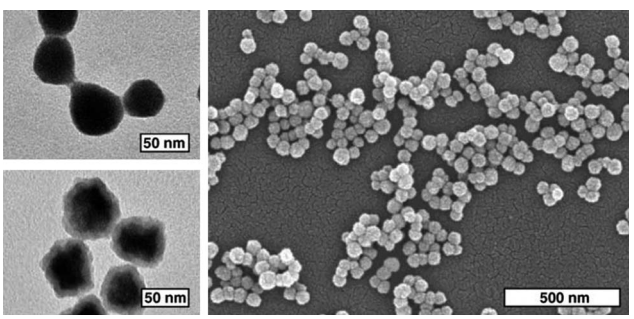

Fig. 11 TEM micrographs of disuccinatocisplatin (DSCP)-loaded nanoMOFs (top left). TEM (right) and SEM (bottom left) micrographs of silica coated DSCP nanoMOF particles. Reprinted from ref. 100 with permission from Elsevier.

5.2 MOF-on-MOF heteroepitaxy

The concept of MOF surface modification and protection can be taken to a higher level by precisely controlling the interfacial interactions between core and shell, that is, by epitaxial growth of the shell material on a well defined single crystal MOF core. This modified core–shell concept has been cast into a creative MOF-on-MOF growth scheme developed by Kitagawa and co-workers, which allows for the design of single-crystal MOF heterostructures with spatially modulated composition, porosity and, hence, functionality.[101–103] These growth schemes have so far been demonstrated only based on micron-scale MOF single crystals and hence fall outside the nanoMOF focus adhered to in this review. Nevertheless, such aesthetic MOF@MOF architectures deserve to be discussed in some detail as they offer, in principle, a generic scheme for the design of multifunctional MOF heterostructures with spatial control of the composition down to the nanoscale.

The hybridization of a MOF core single crystal by epitaxial growth of a single crystalline shell with different structural and porosity properties has been demonstrated successfully based on the archetypal series of tetragonal layer-pillar MOFs with formula $\{M_2(\text{dicarboxylate})_2(\text{diamine})\}_n$.[102] The authors convincingly demonstrate the implementation of well-resolved, spatially separated functionality by the presence of core and shell MOFs with distinct framework topologies and pore surfaces. For example, sequential functionalization was achieved by growing a $\{Zn_2(adc)_2(dabco)\}_n$ shell (adc = 9,10-anthracene dicarboxylate) on top of a $\{Zn_2(bdc)_2\text{-}(dabco)\}_n$ core framework, resulting in heterostructures featuring size selective uptake of bulky hydrocarbons owing to the small apertures of the shell crystal and high storage capacities owing to the large pore volume of the core crystal.

The scope of framework topologies was extended by Koh *et al.* who were able to grow various core–shell architectures of the isoreticular cubic MOF-5 and IRMOF-3 using MOF-on-MOF heteroepitaxy.[104]

The compatibility of both linkers was demonstrated by immersing single crystals of MOF-5 into a growth solution containing the IRMOF-3 building blocks, yielding crystals with a colorless core and an orange shell on the outer side (Fig. 12, left), and *vice versa* (Fig. 12, right). Quite evidently, the heteroepitaxial growth scheme is well transferable to planar systems such as MOF thin films, if the lattice parameters and in-plane connecting groups are identical, as Wöll and co-workers could show by growing $[Zn_2(ndc)_2(dabco)]$ on $[Cu_2(ndc)_2(dabco)]$ crystals *via* the LPE procedure.[85]

This modular synthesis scheme holds great promise for the judicious and spatially well-defined integration of various functionalities in one single, yet heterogeneous MOF monolith, without sacrificing desired properties of the core framework, such as high surface area and pore volume.

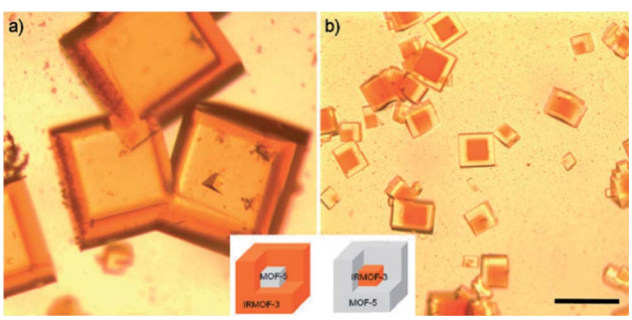

Fig. 12 Optical micrographs of core–shell MOFs: (a) IRMOF-3(shell)@MOF-5(core) and (b) MOF-5(shell)@IRMOF-3(core). Scale bar: 200 μm.[104] Reproduced by permission of The Royal Society of Chemistry.

6. Mechanistic insights and dimension control—a case study

As outlined in the previous chapters, the variety of nanomorphologies that has been synthesized to date is impressive, as is the variety of synthetic methodologies employed. Since a deeper insight into the nucleation and growth stages of nanoMOF formation is pivotal for the directed design of particular nanomorphologies, the complexity of the parameter space in nanoMOF synthesis necessitates radical simplification, and *in situ* techniques adept at monitoring the early stages of nucleation and growth need to be made available. Equally important though, the diversity of systems studied may complicate the elaboration of common underlying themes in the growth mechanisms of different MOF systems. Therefore, rational access to MOF nanomorphologies should be gained by exploring a sufficiently representative system in all its facets, and by subsequently transferring generally applicable motifs to other, more complex systems.

Owing to their stability, ease of synthesis, and rather straightforward solution chemistry, zeolitic imidazolate frameworks (ZIFs), a subclass of MOFs and already among the "drosophilas" in MOF science, lend themselves very well as model systems for an in-depth study of controlling morphology and crystal growth.[6,15,26,105–109]

Both ZIF-8 and ZIF-7, first synthesized by Yaghi and co-workers, are composed of Zn ions joined by imidazolate ligands (ZIF-8: 2-methylimidazole (*mim*) and ZIF-7: benzimidazole (*bim*)).[110] The frameworks with composition $Zn(mim/bim)_2$ are composed of zeolite-like tetrahedral nets with sodalite topology owing to the geometrical similarity between Zn–*mim*/*bim*–Zn and Si–O–Si bond angles. Whereas ZIF-8 crystallizes in the cubic space group $I\bar{4}3m$ and hence is expected to form isotropic nanocrystals, ZIF-7 (hexagonal, space group $R\bar{3}$) features an anisotropic channel network and therefore is ideally suited to study not only the size, but also shape selective synthesis of ZIF-7 nanocrystals. In the following, we will briefly discuss the insights recently gained into the growth mechanism of ZIF-8 nanocrystals and complete this review by surveying recent achievements in the shape-selective synthesis of ZIF-7 nanomorphologies.

6.1 Growth mechanism of ZIF-8 nanoparticles

The first steps toward ZIF-8 nanoparticles were made in the seminal work by Wiebcke and co-workers, who were able to synthesize ZIF-8 nanoparticles of ~45 nm with a narrow size distribution in a room temperature synthesis by adding the bridging ligand 2-methylimidazole (*Hmim*) in eightfold excess with respect to the Zn source.[36] This protocol was later on refined

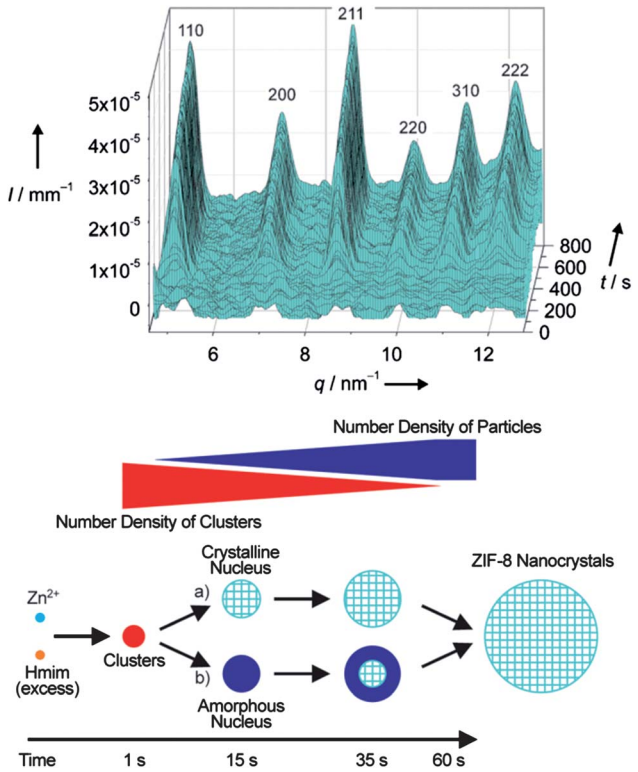

Fig. 13 Top: time resolved WAXS pattern during the formation of ZIF-8 nanocrystals between 1 s and 800 s. The time interval between succeeding patterns is 1 s. Bottom: species occurring during nucleation and growth of ZIF-8 nanocrystals under conditions of high supersaturation. Two possible alternative crystallization pathways (a) and (b) are considered. Reprinted with permission from ref. 58. Copyright© 2011 by John Wiley & Sons, Inc.

by the addition of modulating ligands that modify both coordination and deprotonation equilibria during nucleation and growth, thereby liberating the "active" linker methylimidazolate.[35] Interestingly, although extremely small ZIF-8 nanocrystals (<10 nm) were obtained in the presence of *n*-butylamine, the authors concluded that the most efficient size limiting effect is exerted by the bridging ligand, whose concentration must be high. The ZIF-8 growth process without modulating ligand (solution composition Zn/*Hmim*/MeOH = 1 : 4 : 1000) was monitored by time-resolved *in situ* static light scattering (SLS) and SEM.[35] Careful correlation between the time-dependent size and number distribution of the solution species with the particles observed *ex situ* confirms that ZIF-8 nucleation is continuous and comparatively slow, whereas crystal growth is rapid in the early stages of nanocrystal formation. A similar nucleation-controlled crystallization behaviour with continuous formation of nucleation sites over the timescale of minutes has been observed in other systems such as HKUST-1, studied by *in situ* WAXS and light scattering.[111,112] Somewhat unintuitively, for ZIF-8 a narrowing of the particle size distribution is evident after 1 h, resulting in rather monodisperse particles with an average size of 40 nm. The observed size focusing is rationalized by the termination of fast particle growth at a radius of gyration around 20 nm, which in turn is attested to colloidal stabilization of the primary particles by surface-attached *Hmim* ligands, in line with the measured zeta potential of $\xi = +55$ mV. Although size defocusing by Ostwald ripening subsequently broadens the particle size distribution, rhombic dodecahedral nanoparticles of only 65 nm are obtained even after a reaction time as long as 24 h at RT.

Complementary *in situ* SAXS/WAXS studies on ZIF-8 nucleation and growth by Cravillon *et al.* (Fig. 13) are largely in line with the previously reported SLS data. Owing to the excellent time resolution, prenucleation clusters of approximately 2 nm in size could be detected, suggesting a rather complex crystallization process familiar from the topologically related class of zeolites. Importantly, periodic ZIF-8 particles are formed after 22 s by a monomer/cluster addition mechanism, but not by coalescence. Finally, an important, yet previously somewhat controversial finding reveals the phase-pure formation of ZIF-8 nanocrystals without passing through another transient crystalline phase.[113]

6.2 Morphology control of ZIF-7 nanostructures

The control of size and shape of ZIF-7 nanocrystals has recently been presented in a comprehensive study by Caro and co-workers. This study nicely demonstrates that particular MOF systems may act as a "morphological chameleon" based on the premise that the reaction parameters are adjusted in a suitable way.[76] For the synthesis of spherical ZIF-7 nanocrystals with uniform sizes tunable between 40 and 140 nm the authors proposed a simple "one-pot" strategy using stoichiometric amounts of zinc nitrate and *bim* (molar ratio 1 : 2) in a polyethyleneimine–dimethylformamide (PEI–DMF) solution at room temperature (Fig. 14, left).[76] PEI is acting as a base for *bim*, thus leading to a high nucleation rate which is critical for the formation of nanoparticles. In order to alter the growth kinetics

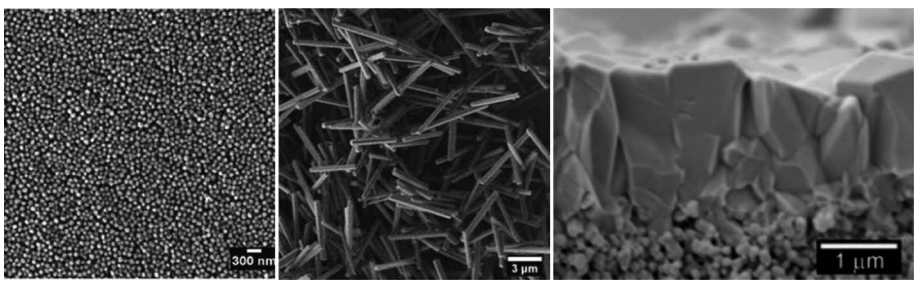

Fig. 14 Nanoparticles synthesized from $Zn(NO_3)_2$ as a metal source (left), nanorods grown in the presence of $ZnCl_2$ (middle), and ZIF-7 membrane on alumina disk (right). Reprinted with permission from ref. 76 and 77. Copyright© 2010 by John Wiley & Sons, Inc.

of the different crystal faces and, hence, increase the aspect ratio of the nanoparticles, the authors employed zinc chloride instead of zinc nitrate as a precursor. As a rationale, the authors invoke the "hard soft acid base" theory (HSAB), which classifies zinc and chloride as "intermediate" acids and bases, respectively, indicating strong interactions between them. Therefore, the differences in growth kinetics of the low index faces, characterized by the attachment energy,[114] will be more distinct in the presence of chloride ions, resulting in enlarged differences in the growth rates of the {003} and {110}/{101} faces and thus, prismatic hexagonal crystals with high aspect ratios (Fig. 14, middle). When adding diethylamine (DEA), the size and aspect ratio of the ZIF-7 crystals could further be adjusted by varying the amount of DEA acting as a deprotonation agent for the *bim* linker. Having established protocols for tailoring the crystal size and morphology, the authors succeeded in growing highly oriented ZIF-7 membranes starting from randomly oriented seed layers, which exhibit a clear morphological relation to the nanorods observed by non-supported growth (Fig. 14, right).

In a previous report by the same authors, the growth of randomly oriented ZIF-7 membranes had been analysed.[77] Permeation measurements through both oriented and non-oriented membrane types demonstrate the gas-separation capabilities of such ZIF films *via* a molecular sieving effect with an increased selectivity at elevated temperatures. Interestingly, the permeance of H_2 was found to be lower for the highly oriented membrane as compared to the randomly oriented layer, which the authors attribute to the anisotropic pore structure, as "neither the pyramidal termination {101} faces nor the prismatic {110} faces of the columnar crystals possess direct entrances for guest molecules."[76] The observed membrane performances further substantiate the efficiency of morphology tuning to enhance the functionality of nanoMOFs and devices made thereof.

7. Conclusion

This feature article has attempted to distil off the essence of state-of-the-art approaches toward nanoscale MOF architectures with different dimensionalities. Recent advances in the field have been highlighted with a particular focus on protocols (a) allowing for a high level of control with respect to composition and structure at the nanoscale, (b) enabling reliable tuning of the nanoscale morphology and, hence, dimensionality, or (c) elaborating conceptually new fabrication strategies to achieve the above goals. Besides, we have gathered insights into the mechanism of nucleation and growth processes in nanoMOF synthesis of representative MOF systems such as ZIF-8, which ultimately may be generalized to other MOF systems and enable a more purposeful fine-tuning of the reaction parameters in nanoMOF synthesis.

While the development of new nanoMOFs has considerably quickened its pace, thanks to a plethora of different synthesis strategies that have significantly matured over the past few years, many of the reported approaches are still essentially trial and error-based. Therefore, many nanoMOFs have been obtained by serendipity rather than rational design, yet a number of encouraging approaches has recently been developed that point toward more directed morphology control. Among these, templating strategies enabling crystallographically oriented growth and interfacial control such as those in microfluidic environments excel by their straightforward concept, yet highly reproducible and tunable size and shape control. Also, the step-by-step liquid layer epitaxy for the immobilization of ultrathin MOF films allows for an unprecedented level of control of composition, topology and film thickness at the nanoscale. However, future MOF nanomorphologies will inevitably gain complexity—hollow and hybrid MOF spheres as well as hierarchically micro–mesoporous MOFs have given us a flavor of what is already possible.

As a perspective, the integration of different functionalities into one "hybrid" MOF platform will be a key asset. Highly oriented MOF-on-MOF heteroepitaxy on planar and curved surfaces has been trendsetting in this respect. Once this technology is adapted to nanofabrication protocols, the stage is set for the design of tailor-made, multifunctional MOFs with spatially distinct porosity and surface properties.

The inherent shape-dependent properties of nanomaterials and the prospect of a vast spectrum of nanoMOF applications, ranging from drug delivery, catalysis and sensing to smart membranes, leave the synthetic chemist with the challenge to create various nanomorphologies of one and the same material. A look into the toolbox of modern nanoscale synthesis may do the trick—the tools are at hand.

Acknowledgements

The authors acknowledge financial support by the Priority Program 1362 "Porous Metal–Organic Frameworks" of the Deutsche Forschungsgemeinschaft (DFG), the Nanosystems Initiative Munich (NIM) and the Center for NanoScience (CeNS).

Dedicated to Professor Wolfgang Beck on the occasion of his 80th birthday.

References

1 J. L. C. Rowsell and O. M. Yaghi, *Microporous Mesoporous Mater.*, 2004, **73**, 3–14.
2 O. M. Yaghi, M. O'Keeffe, N. W. Ockwig, H. K. Chae, M. Eddaoudi and J. Kim, *Nature*, 2003, **423**, 705–714.
3 S. Hausdorf, W. Seichter, E. Weber and F. O. R. L. Mertens, *Dalton Trans.*, 2009, 1107–1113.
4 J.-R. Li, R. J. Kuppler and H.-C. Zhou, *Chem. Soc. Rev.*, 2009, **38**, 1477–1504.
5 C.-Y. Huang, M. Song, Z.-Y. Gu, H.-F. Wang and X.-P. Yan, *Environ. Sci. Technol.*, 2011, **45**, 4490–4496.
6 A. Demessence, C. Boissiere, D. Grosso, P. Horcajada, C. Serre, G. Ferey, G. J. A. A. Soler-Illia and C. Sanchez, *J. Mater. Chem.*, 2010, **20**, 7676–7681.
7 H. Wu, W. Zhou and T. Yildirim, *J. Am. Chem. Soc.*, 2007, **129**, 5314–5315.
8 B. Kesanli, Y. Cui, M. R. Smith, E. W. Bittner, B. C. Bockrath and W. Lin, *Angew. Chem., Int. Ed.*, 2005, **44**, 72–75.
9 H. Bux, A. Feldhoff, J. Cravillon, M. Wiebcke, Y.-S. Li and J. Caro, *Chem. Mater.*, 2011, **23**, 2262–2269.
10 S. R. Venna and M. A. Carreon, *J. Am. Chem. Soc.*, 2009, **132**, 76–78.
11 E. Biemmi, A. Darga, N. Stock and T. Bein, *Microporous Mesoporous Mater.*, 2008, **114**, 380–386.
12 L. E. Kreno, J. T. Hupp and R. P. Van Duyne, *Anal. Chem.*, 2010, **82**, 8042–8046.
13 J. Liu, F. Sun, F. Zhang, Z. Wang, R. Zhang, C. Wang and S. Qiu, *J. Mater. Chem.*, 2011, **21**, 3775–3778.

14 X. Zhang, M. A. Ballem, Z.-J. Hu, P. Bergman and K. Uvdal, *Angew. Chem., Int. Ed.*, 2011, **50**, 5729–5733.
15 Y. Pan, Y. Liu, G. Zeng, L. Zhao and Z. Lai, *Chem. Commun.*, 2011, **47**, 2071–2073.
16 S. Keskin and S. Kizilel, *Ind. Eng. Chem. Res.*, 2011, **50**, 1799–1812.
17 W. Hatakeyama, T. J. Sanchez, M. D. Rowe, N. J. Serkova, M. W. Liberatore and S. G. Boyes, *ACS Appl. Mater. Interfaces*, 2011, **3**, 1502–1510.
18 R. Ananthoji, J. F. Eubank, F. Nouar, H. Mouttaki, M. Eddaoudi and J. P. Harmon, *J. Mater. Chem.*, 2011, **21**, 9587–9594.
19 J. Della Rocca, D. Liu and W. Lin, *Acc. Chem. Res.*, 2011, **44**, 957–968.
20 D. Zhao, S. Tan, D. Yuan, W. Lu, Y. H. Rezenom, H. Jiang, L.-Q. Wang and H.-C. Zhou, *Adv. Mater.*, 2010, **23**, 90–93.
21 H.-L. Jiang and Q. Xu, *Chem. Commun.*, 2011, **47**, 3351–3370.
22 W. Lin, W. J. Rieter and K. M. L. Taylor, *Angew. Chem., Int. Ed.*, 2009, **48**, 650–658.
23 A. Corma, H. Garcia and F. X. Llabresi Xamena, *Chem. Rev.*, 2010, **110**, 4606–4655.
24 G. Nickerl, A. Henschel, R. Grünker, K. Gedrich and S. Kaskel, *Chem. Ing. Tech.*, 2010, **83**, 90–103.
25 F. Fajula, A. Galarneau and F. D. Renzo, *Microporous Mesoporous Mater.*, 2005, **82**, 227–239.
26 G. Lu and J. T. Hupp, *J. Am. Chem. Soc.*, 2010, **132**, 7832–7833.
27 J. Wang, J. D. Byrne, M. E. Napier and J. M. DeSimone, *Small*, 2011, **7**, 1919–1931.
28 H. B. Na, I. C. Song and T. Hyeon, *Adv. Mater.*, 2009, **21**, 2133–2148.
29 R. E. Morris, *Nat. Chem.*, 2011, **3**, 347–348.
30 N. Fukao, K.-H. Kyung, K. Fujimoto and S. Shiratori, *Macromolecules*, 2011, **44**, 2964–2969.
31 A. M. Spokoyny, D. Kim, A. Sumrein and C. A. Mirkin, *Chem. Soc. Rev.*, 2009, **38**, 1218–1227.
32 O. Shekhah, J. Liu, R. A. Fischer and C. Woll, *Chem. Soc. Rev.*, 2011, **40**, 1081–1106.
33 T. Tsuruoka, S. Furukawa, Y. Takashima, K. Yoshida, S. Isoda and S. Kitagawa, *Angew. Chem., Int. Ed.*, 2009, **48**, 4739–4743.
34 P. Horcajada, C. Serre, D. Grosso, C. Boissière, S. Perruchas, C. Sanchez and G. Férey, *Adv. Mater.*, 2009, **21**, 1931–1935.
35 J. Cravillon, R. Nayuk, S. Springer, A. Feldhoff, K. Huber and M. Wiebcke, *Chem. Mater.*, 2011, **23**, 2130–2141.
36 J. Cravillon, S. Munzer, S.-J. Lohmeier, A. Feldhoff, K. Huber and M. Wiebcke, *Chem. Mater.*, 2009, **21**, 1410–1412.
37 N. A. Khan, I. J. Kang, H. Y. Seok and S. H. Jhung, *Chem. Eng. J.*, 2011, **166**, 1152–1157.
38 L.-G. Qiu, Z.-Q. Li, Y. Wu, W. Wang, T. Xu and X. Jiang, *Chem. Commun.*, 2008, 3642–3644.
39 Z.-Q. Li, L.-G. Qiu, W. Wang, T. Xu, Y. Wu and X. Jiang, *Inorg. Chem. Commun.*, 2008, **11**, 1375–1377.
40 S. Diring, S. Furukawa, Y. Takashima, T. Tsuruoka and S. Kitagawa, *Chem. Mater.*, 2010, **22**, 4531–4538.
41 Z. Ni and R. I. Masel, *J. Am. Chem. Soc.*, 2006, **128**, 12394–12395.
42 Z.-Q. Li, L.-G. Qiu, T. Xu, Y. Wu, W. Wang, Z.-Y. Wu and X. Jiang, *Mater. Lett.*, 2009, **63**, 78–80.
43 K. S. Suslick, *Ultrasound: Its Chemical, Physical and Biological Effects*, VCH, Weinheim, Germany, 1988.
44 K. S. Suslick, *Science*, 1990, **247**, 1439–1445.
45 K. Baba, H. Kasai, S. Okada, H. Oikawa and H. Nakanishi, *Opt. Mater.*, 2003, **21**, 591–594.
46 C. Nitschke, S. M. O'Flaherty, M. Kröll and W. J. Blau, *J. Phys. Chem. B*, 2003, **108**, 1287–1295.
47 E. Haque, N. A. Khan, J. H. Park and S. H. Jhung, *Chem.–Eur. J.*, 2010, **16**, 1046–1052.
48 M. Schlesinger, S. Schulze, M. Hietschold and M. Mehring, *Microporous Mesoporous Mater.*, 2011, **132**, 121–127.
49 Z. Xiang, D. Cao, X. Shao, W. Wang, J. Zhang and W. Wu, *Chem. Eng. Sci.*, 2010, **65**, 3140–3146.
50 N. A. Khan, E. Haque and S. H. Jhung, *Phys. Chem. Chem. Phys.*, 2010, **12**, 2625–2631.
51 T. Chalati, P. Horcajada, R. Gref, P. Couvreur and C. Serre, *J. Mater. Chem.*, 2011, **21**, 2220–2227.
52 Y. Zhao, J. Zhang, B. Han, J. Song, J. Li and Q. Wang, *Angew. Chem., Int. Ed.*, 2011, **50**, 636–639.
53 J. Liu, S. Cheng, J. Zhang, X. Feng, X. Fu and B. Han, *Angew. Chem., Int. Ed.*, 2007, **46**, 3313–3315.
54 K. P. Johnston, K. L. Harrison, M. J. Clarke, S. M. Howdle, M. P. Heitz, F. V. Bright, C. Carlier and T. W. Randolph, *Science*, 1996, **271**, 624–626.
55 R. Ameloot, F. Vermoortele, W. Vanhove, M. B. J. Roeffaers, B. F. Sels and D. E. De Vos, *Nat. Chem.*, 2011, **3**, 382–387.
56 H. Guo, Y. Zhu, S. Qiu, J. A. Lercher and H. Zhang, *Adv. Mater.*, 2010, **22**, 4190–4192.
57 D. Zacher, R. Schmid, C. Wöll and R. A. Fischer, *Angew. Chem., Int. Ed.*, 2011, **50**, 176–199.
58 J. Cravillon, C. A. Schröder, R. Nayuk, J. Gummel, K. Huber and M. Wiebcke, *Angew. Chem., Int. Ed.*, 2011, **50**, 8067–8071.
59 Q. Shi, Z. Chen, Z. Song, J. Li and J. Dong, *Angew. Chem., Int. Ed.*, 2010, **50**, 672–675.
60 A. G. Wong-Foy, A. J. Matzger and O. M. Yaghi, *J. Am. Chem. Soc.*, 2006, **128**, 3494–3495.
61 M. Eddaoudi, J. Kim, N. Rosi, D. Vodak, J. Wachter, M. O'Keeffe and O. M. Yaghi, *Science*, 2002, **295**, 469–472.
62 T. M. Reineke, M. Eddaoudi, M. Fehr, D. Kelley and O. M. Yaghi, *J. Am. Chem. Soc.*, 1999, **121**, 1651–1657.
63 W. J. Rieter, K. M. L. Taylor, H. An, W. Lin and W. Lin, *J. Am. Chem. Soc.*, 2006, **128**, 9024–9025.
64 K. M. L. Taylor, A. Jin and W. Lin, *Angew. Chem., Int. Ed.*, 2008, **47**, 7722–7725.
65 K. M. L. Taylor, W. J. Rieter and W. Lin, *J. Am. Chem. Soc.*, 2008, **130**, 14358–14359.
66 K. P. Brazhnik, W. N. Vreeland, J. B. Hutchison, R. Kishore, J. Wells, K. Helmerson and L. E. Locascio, *Langmuir*, 2005, **21**, 10814–10817.
67 A. L. Thangawng, P. B. Howell, Jr, J. J. Richards, J. S. Erickson and F. S. Ligler, *Lab Chip*, 2009, **9**, 3126–3130.
68 J. Puigmartí-Luis, D. Schaffhauser, B. R. Burg and P. S. Dittrich, *Adv. Mater.*, 2010, **22**, 2255–2259.
69 J. Puigmarti-Luis, M. Rubio-Martinez, U. Hartfelder, I. Imaz, D. Maspoch and P. S. Dittrich, *J. Am. Chem. Soc.*, 2011, **133**, 4216–4219.
70 Q. Zhang, S.-J. Liu and S.-H. Yu, *J. Mater. Chem.*, 2009, **19**, 191–207.
71 M. Jahan, Q. Bao, J.-X. Yang and K. P. Loh, *J. Am. Chem. Soc.*, 2010, **132**, 14487–14495.
72 S. Ma and H.-C. Zhou, *Chem. Commun.*, 2010, **46**, 44–53.
73 M. Eddaoudi, H. Li and O. M. Yaghi, *J. Am. Chem. Soc.*, 2000, **122**, 1391–1397.
74 D. Zacher, A. Baunemann, S. Hermes and R. A. Fischer, *J. Mater. Chem.*, 2007, **17**, 2785–2792.
75 S. Hermes, F. Schröder, R. Chelmowski, C. Wöll and R. A. Fischer, *J. Am. Chem. Soc.*, 2005, **127**, 13744–13745.
76 Y.-S. Li, H. Bux, A. Feldhoff, G.-L. Li, W.-S. Yang and J. Caro, *Adv. Mater.*, 2010, **22**, 3322–3326.
77 Y.-S. Li, F.-Y. Liang, H. Bux, A. Feldhoff, W.-S. Yang and J. Caro, *Angew. Chem., Int. Ed.*, 2010, **49**, 548–551.
78 R. Ameloot, L. Pandey, M. Van der Auweraer, L. Alaerts, B. F. Sels and D. E. De Vos, *Chem. Commun.*, 2010, **46**, 3735–3737.
79 M. Kind and C. Wöll, *Prog. Surf. Sci.*, 2009, **84**, 230–278.
80 A. Schoedel, C. Scherb and T. Bein, *Angew. Chem., Int. Ed.*, 2010, **49**, 7225–7228.
81 O. Shekhah, H. Wang, S. Kowarik, F. Schreiber, M. Paulus, M. Tolan, C. Sternemann, F. Evers, D. Zacher, R. A. Fischer and C. Wöll, *J. Am. Chem. Soc.*, 2007, **129**, 15118–15119.
82 O. Shekhah, H. Wang, M. Paradinas, C. Ocal, B. Schupbach, A. Terfort, D. Zacher, R. A. Fischer and C. Woll, *Nat. Mater.*, 2009, **8**, 481–484.
83 G. Decher, J. D. Hong and J. Schmitt, *Thin Solid Films*, 1992, **210**, 831–835.
84 H. K. Arslan, O. Shekhah, J. Wohlgemuth, M. Franzreb, R. A. Fischer and C. Wöll, *Adv. Funct. Mater.*, 2011, **21**, 4228–4231.
85 O. Shekhah, K. Hirai, H. Wang, H. Uehara, M. Kondo, S. Diring, D. Zacher, R. A. Fischer, O. Sakata, S. Kitagawa, S. Furukawa and C. Wöll, *Dalton Trans.*, 2011, 4954–4958.
86 D. Zacher, K. Yusenko, A. Bétard, S. Henke, M. Molon, T. Ladnorg, O. Shekhah, B. Schüpbach, T. de los Arcos, M. Krasnopolski, M. Meilikhov, J. Winter, A. Terfort, C. Wöll and R. A. Fischer, *Chem.–Eur. J.*, 2011, **17**, 1448–1455.
87 O. Shekhah, H. Wang, D. Zacher, R. A. Fischer and C. Wöll, *Angew. Chem., Int. Ed.*, 2009, **48**, 5038–5041.

88 P.-Z. Li, Y. Maeda and Q. Xu, *Chem. Commun.*, 2011, **47**, 8436–8438.
89 D. Zacher, O. Shekhah, C. Woll and R. A. Fischer, *Chem. Soc. Rev.*, 2009, **38**, 1418–1429.
90 A. Demessence, P. Horcajada, C. Serre, C. Boissiere, D. Grosso, C. Sanchez and G. Ferey, *Chem. Commun.*, 2009, 7149–7151.
91 H. Li, M. Eddaoudi, T. L. Groy and O. M. Yaghi, *J. Am. Chem. Soc.*, 1998, **120**, 8571–8572.
92 B. F. Hoskins and R. Robson, *J. Am. Chem. Soc.*, 1990, **112**, 1546–1554.
93 W. J. Rieter, K. M. L. Taylor and W. Lin, *J. Am. Chem. Soc.*, 2007, **129**, 9852–9853.
94 M. D. Rowe, D. H. Thamm, S. L. Kraft and S. G. Boyes, *Biomacromolecules*, 2009, **10**, 983–993.
95 K. M. L. Taylor-Pashow, J. D. Rocca, Z. Xie, S. Tran and W. Lin, *J. Am. Chem. Soc.*, 2009, **131**, 14261–14263.
96 K. K. Tanabe, Z. Wang and S. M. Cohen, *J. Am. Chem. Soc.*, 2008, **130**, 8508–8517.
97 R. C. Huxford, J. Della Rocca and W. Lin, *Curr. Opin. Chem. Biol.*, 2010, **14**, 262–268.
98 M. Vallet-Regí, F. Balas and D. Arcos, *Angew. Chem., Int. Ed.*, 2007, **46**, 7548–7558.
99 P. Horcajada, T. Chalati, C. Serre, B. Gillet, C. Sebrie, T. Baati, J. F. Eubank, D. Heurtaux, P. Clayette, C. Kreuz, J.-S. Chang, Y. K. Hwang, V. Marsaud, P.-N. Bories, L. Cynober, S. Gil, G. Ferey, P. Couvreur and R. Gref, *Nat. Mater.*, 2010, **9**, 172–178.
100 R. C. Huxford, J. Della Rocca and W. Lin, *Curr. Opin. Chem. Biol.*, 2010, **14**, 262–268.
101 S. Furukawa, K. Hirai, K. Nakagawa, Y. Takashima, R. Matsuda, T. Tsuruoka, M. Kondo, R. Haruki, D. Tanaka, H. Sakamoto, S. Shimomura, O. Sakata and S. Kitagawa, *Angew. Chem., Int. Ed.*, 2009, **48**, 1766–1770.
102 S. Furukawa, K. Hirai, Y. Takashima, K. Nakagawa, M. Kondo, T. Tsuruoka, O. Sakata and S. Kitagawa, *Chem. Commun.*, 2009, 5097–5099.
103 K. Hirai, S. Furukawa, M. Kondo, H. Uehara, O. Sakata and S. Kitagawa, *Angew. Chem., Int. Ed.*, 2011, **50**, 8057–8061.
104 K. Koh, A. G. Wong-Foy and A. J. Matzger, *Chem. Commun.*, 2009, 6162–6164.
105 J. Yao, D. Dong, D. Li, L. He, G. Xu and H. Wang, *Chem. Commun.*, 2011, **47**, 2559–2561.
106 L. Hertäg, H. Bux, J. Caro, C. Chmelik, T. Remsungnen, M. Knauth and S. Fritzsche, *J. Membr. Sci.*, 2011, **377**, 36–41.
107 Y. Liu, E. Hu, E. A. Khan and Z. Lai, *J. Membr. Sci.*, 2010, **353**, 36–40.
108 T. D. Bennett, J.-C. Tan, S. A. Moggach, R. Galvelis, C. Mellot-Draznieks, B. A. Reisner, A. Thirumurugan, D. R. Allan and A. K. Cheetham, *Chem.–Eur. J.*, 2010, **16**, 10684–10690.
109 W. Morris, C. J. Doonan, H. Furukawa, R. Banerjee and O. M. Yaghi, *J. Am. Chem. Soc.*, 2008, **130**, 12626–12627.
110 K. S. Park, Z. Ni, A. P. Côté, J. Y. Choi, R. Huang, F. J. Uribe-Romo, H. K. Chae, M. O'Keeffe and O. M. Yaghi, *Proc. Natl. Acad. Sci. U. S. A.*, 2006, **103**, 10185–10191.
111 F. Millange, M. I. Medina, N. Guillou, G. Férey, K. M. Golden and R. I. Walton, *Angew. Chem., Int. Ed.*, 2009, **49**, 763–766.
112 D. Zacher, J. Liu, K. Huber and R. A. Fischer, *Chem. Commun.*, 2009, 1031–1033.
113 S. R. Venna, J. B. Jasinski and M. A. Carreon, *J. Am. Chem. Soc.*, 2010, **132**, 18030–18033.
114 P. Hartman and W. G. Perdok, *Acta Crystallogr.*, 1955, **8**, 525–529.